*J. Basic. Appl. Sci. Res.*, 3(11)230-250, 2013



ISSN 2090-4304
**Journal of Basic and Applied Scientific Research**
*www.textroad.com*

# Effect of Dual-Phase-Lag in the Presence of Suction/Injection on Unsteady Free-Convection Micro-Channel Flow between Two Vertical Porous Plates

**[1]B. K. Jha, [1] C. O. Obieje and [2]Ahmed Kadhim Hussein**

[1]Mathematics Department, Ahmadu Bello University, Zaria, Kaduna State, Nigeria
[2,*]College of Engineering, Department of Mechanical Engineering, Babylon University, Babylon City, Hilla, Iraq

*Received: August 3 2013*
*Accepted: September 12 2013*

## ABSTRACT

The transient, laminar, fully developed, free convection flow inside an open-ended, vertical, parallel-porous-plate, micro-channel is considered using Dual-Phase-Lag heat conduction model. This study adopted the approach of the model that combines both continuum and possibility of slip at the boundary. The well known Laplace transform technique is applied to solve the time dependent governing equations, while the method of Riemann-sum approximation is employed to invert the Laplace domain to the time domain in order to obtain the velocity, temperature, skin-friction and rate of heat transfer. The obtained results are described by line graphs. It has been observed that the phase lags in both heat flux and temperature gradient on the micro-channel thermal behaviour have significant effect at the early stage of time. And as the temperature phase lag is set greater than that of heat flux phase lag, higher fluid temperature, velocity as well as the velocity slip at the hot wall are observed than when it is less than the heat flux phase lag. Increase in suction/injection increases the skin friction and the Nusselt number at the hot wall of the micro-channel.

**KEY WORDS:** micro-channel, transient flow, dual-phase-lag, porous plate, suction/injection

## 1. INTRODUCTION

Microfluidics has become an emerging science and technology of systems that process or manipulate small amount of fluids, using channels with dimensions of tens to hundreds of micrometres. Due to the minute length scale characterising microchannels, the Knudsen number ($Kn = \lambda/L$, ratio between the gas mean free path and the length scale) determine the behaviour of fluid flow. Microelectronic devices generate heat as a result of the electrical activity of the internal circuitry. In order to minimize the damaging effects of this heat, thermal management systems have been developed to remove the heat. There is a growing interest in micro-channel fluid mechanics and heat transfer resulting from the rapid growth of novel techniques applied in microelectro mechanical systems (MEMS). These applications of micro-channel heat transfer include: cooling of high power density microchips in the CPU systems, manufacturing and material processing operations, transportation of fluids for chemical and biological processing, biomedical applications such as drug delivery, DNA sequencing and bio-MEMS. As a result, so many models have been proposed to take into account the finite speed of heat propagation and its effects on the MEMS. These models include the Hyperbolic heat conduction and the Dual-phase-lag models which describe heat conduction as wave, against the diffusion model presented by Fourier's law.

The Dual-Phase-Lag (DPL) was first proposed by Tzou ([1], [2]) when he considered the effect of finite relaxation time by using the heat flux and temperature phase lags. The relaxation time was said to have been caused by micro structural interaction like phonon to phonon collisions, while the phase lag is interpreted as the relaxation time due to fast-transient effects of the thermal inertia Quintanilla & Rache, [3]). Cattaneo [4] and Vernotte, [5] suggested independently a modified heat flow in the form

$$\vec{q}\left(t + \tau_q, \vec{r}\right) = -K\vec{\nabla}T(t, \vec{r}) \quad (1)$$

Equation (1) represents a total departure from the Fourier heat conduction model. It also suggests a model which assumes that heat flux vector (the effect) and the temperature gradient (the cause) across a material volume occur at different instants of time; referring the time delay between the heat flux and the temperature gradient as the relaxation time $\tau_q$. According to the proposal presented by Tzou in 1995, we have the following as modification to eqn. (1):

$$\vec{q}\left(t + \tau_q, \vec{r}\right) = -K\vec{\nabla}T(t + \tau_T, \vec{r}) \quad (2)$$

The equation (2) proposes a non-Fourier approximation for heat conduction in which the heat flux vector at a point in the material at time $t + \tau_q$, corresponds to the temperature gradient at the same point at the time $t + \tau_T$. The terms $\tau_q$ and $\tau_T$ represent respectively the heat flux phase lag and the temperature gradient phase lag; popularly referred to as Dual-phase-lag (DPL). This model however, allows either the temperature gradient (the cause) to precede the heat flux vector (the effect) or the heat flux vector (the cause) to precede the temperature

[*]**Corresponding Author:** Ahmed Kadhim Hussein, College of Engineering, Department of Mechanical Engineering, Babylon University, Babylon City, Hilla, Iraq. (ahmedkadhim7474@gmail.com)

gradient (the effect) in the transient process (Al-Nimr & Naji, [6, 7]). The studies on hyperbolic heat conduction equation in an Anisotropic material and the phase-lag effect on entropy production show that when $\tau_T > \tau_q$, the temperature gradient in the material is the resultant effect of the heat flow, making the heat flux vector the cause and the temperature gradient the effect. When $\tau_q > \tau_T$, then, the heat flow is motivated by the temperature gradient which makes the heat flux vector the effect and the temperature gradient as the cause.

It has been noted that due to the lagging responses in both hyperbolic and dual-phase-lag heat-conduction models; much attention has been given to these areas than the classical diffusion model [8]. Hyperbolic and DPL heat conduction have found utilization in several cases ([2], [9]). For instance, Al-Nimr and Khadrawi [10], used DPL heat conduction model to investigate the thermal behaviour of stagnant gas which was confined in a horizontal micro-channel. The effects of relaxation time $\tau_q$, the thermal retardation time $\tau_T$, as well as the Knudsen number in the micro-channel behaviour were investigated. It was found that the deviation between the predictions presented by the parabolic and that of hyperbolic models are insignificant. This work further established that the predictions of parabolic and DPL models are significant within the same operating conditions. Another interesting investigation was the one carried out by Ghazanfarian and Abbassi [11]; which used DPL conduction model with new boundary condition to simulate nano-scale and micro-scale heat conduction. This work was able to establish the accuracy of the DPL conduction model by comparing the results obtained from the Ballistic-Diffusive equation [12] with Boltzmann equation [13]. Khadrawi and Al-Nimr [8] investigation was on DPL heat conduction model in unsteady natural convection fluid flow in a vertical micro-channel. They concluded that the effect of the phase lags was to increase the slip in the hydrodynamic behaviour. Several other researches on DPL conduction model carried out as observed in the availuable literature also include the work of Quintanilla, [14]; Basirat *et al*., [15]; and Horgan & Quatanilla, [16].

The present study is investigating the micro-channel transient thermal and hydrodynamic behaviour under the effect of dual-phase-lag heat-conduction model with suction/injection at the boundary walls. The investigation is adopting the model that combines the continuum approach with slip at the boundaries. The perturbation in the micro-channel unsteady thermal characteristics due to the suction/injection at the porous walls, phase-lag in heat flux, the phase-lag in temperature gradients and the Knudsen number are investigated with their roles on the heat transfer at the channel walls.

## 2. ANALYSIS

The transient, laminar, fully developed, free convection flow inside an open-ended, vertical, parallel-porous-plate, micro-channel is considered. The fluid is assumed to be Newtonian with uniform properties and that both viscous dissipation and internal heat generation are absent. The application of suction and injection occur simultaneously at the respective plates as shown in Fig. 1.

The governing equations of the hydrodynamic and thermal behaviour, as described by the dual-phase-lag heat-conduction model, are given as Tzou, [1, 2]; Al-Nimr & Naji, [6, 7]; and Khadrawi & Al-Nimr,[ 8]:

$$\frac{\partial u}{\partial t} + s\frac{\partial u}{\partial y} = P_r\frac{\partial^2 u}{\partial y^2} + T \tag{3}$$

$$\frac{\partial T}{\partial t} + s\frac{\partial T}{\partial y} = -\frac{\partial Q}{\partial y} \tag{4}$$

$$\tau_q\frac{\partial Q}{\partial t} + Q = -\left[\tau_T\frac{\partial^2 T}{\partial y \partial t} + \frac{\partial T}{\partial y}\right] \tag{5}$$

Equations (3) – (5) assume the following initial thermal boundary conditions

$$T(0,y) = u(0,y) = 0 \tag{6a}$$

$$T(0,t) = r_t + \frac{kn}{P_r}\Psi\frac{\partial T}{\partial y}\Big|_{y=0} \tag{6b}$$

$$T(1,t) = 1 - \frac{kn}{P_r}\Psi\frac{\partial T}{\partial y}\Big|_{y=1} \tag{6c}$$

$$u(0,t) = +\Omega\frac{kn}{P_r}\frac{\partial U}{\partial y}\Big|_{y=0} \tag{6d}$$

$$u(1,t) = -\Omega\frac{kn}{P_r}\frac{\partial U}{\partial y}\Big|_{y=1} \tag{6e}$$

Also, the dimensionless slip-flow and thermal-jump boundary conditions are given respectively;

$$\Delta u|_{hot\ wall} = u(1,t) = -\Omega\frac{kn}{P_r}\frac{\partial u}{\partial y}(1,t),$$

$$\Delta T|_{cold\ wall} = T(0,t) - r_t = \frac{kn}{P_r}\Psi\frac{\partial T}{\partial y}(0,t)$$

$$\Delta T|_{hot\ wall} = T(1,t) - 1 = -\frac{kn}{P_r}\Psi\frac{\partial T}{\partial y}(1,t)$$

Where *Pr* is the Prandtl number which is inversely proportional to the thermal diffusivity of the working fluid; the term $\Omega = \frac{2-\sigma_v}{\sigma_v}$ is the ratio of the tangential momentum accommodation, and $\Psi = \frac{2-\sigma_T}{\sigma_T}.\frac{2\gamma}{\gamma+1}$ is the ratio of the tangential thermal accommodation. Both ratios are considered for the purpose of this study as 1, to enable fluid molecules reflect at random angles hence, lose all their tangential momentum (i.e. $\sigma_T \to 1$). This offers a realistic engineering application domain [18]. The term $s$ is the dimensionless suction/injection velocity. When $s > 0$, we have injection at the porous plate $y = 0$ and corresponding suction at plate $y = 1$ ; while $s < 0$ implies that suction occurs at plate $y = 0$ with corresponding injection on the other plate. The right-hand side of equations (6c) and (6e) represent the slip in the hydrodynamic and thermal conditions of the boundary. However the non-dimensional quantities in the equations above are listed in the nomenclature and the schematic diagram of the problem is shown in figure 1.

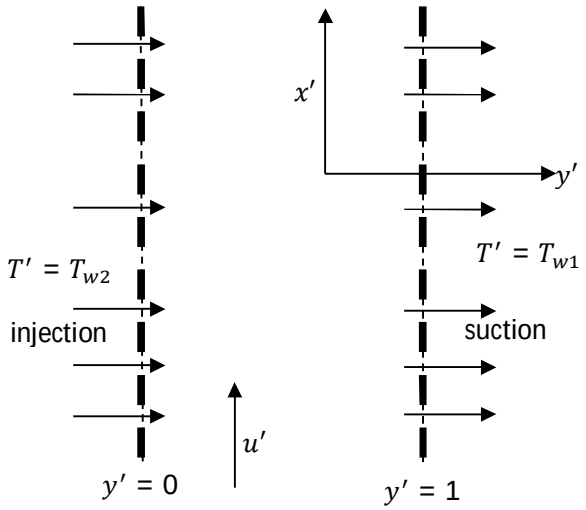


Fig. 1. Schematic diagram of the problem.

khadrawi and Al-Nimr [8] observed that $\tau_T$ and $\tau_q$ may have significant effect on the microchannel thermal behaviour within the very early stage of time, i.e., $t \ll \tau_T$ and $t \ll \tau_q$. This is shown clearly when equation (5) is rewritten in the following form:

$$\frac{\partial Q}{\partial\left(\frac{t}{\tau_q}\right)} + Q = -\left[\frac{\partial^2 T}{\partial y \partial\left(\frac{t}{\tau_T}\right)} + \frac{\partial T}{\partial y}\right] \tag{6f}$$

Where the first and the third terms will have significant effect if $\left(\frac{t}{\tau_q}\right) \ll 1$ and $\left(\frac{t}{\tau_T}\right) \ll 1$.

The Laplace transformation technique is used to solve the equations (3), (4), and (5) with the following notations:

$$L\{T(y,t)\} = W(y,p);\ L\{Q(y,t)\} = V(y,p);\ and\ L\{U(y,t)\} = F(y,p).$$

The three equations are in Laplace transformation forms as follow;

$$p\tau_q W(y,p) + s\frac{dW}{dy} = -\frac{dV}{dy} \tag{7}$$

$$pF(y,p) + s\frac{dF}{dy} = P_r\frac{d^2F}{dy^2} + W(y,p) \tag{8}$$

$$p\tau_q V(y,p) + V(y,p) = -\left[p\tau_T\frac{dW}{dy} + \frac{dW}{dy}\right] \tag{9}$$

Also the Laplace transformation of the boundary conditions are given as

$$W(0,p) = \frac{r_t}{p} + \frac{kn}{P_r}\frac{dW}{dY}\Big|_{y=0} \tag{10a}$$

$$W(1,p) = \frac{1}{p} - \frac{kn}{P_r}\frac{dW}{dY}\Big|_{y=1} \tag{10b}$$

$$F(0,p) = \frac{kn}{P_r}\frac{dF}{dY}|_{y=0} \quad (10c)$$

$$F(1,p) = -\frac{kn}{P_r}\frac{dF}{dY}|_{y=1} \quad (10d)$$

From Eq. (9), we obtain the following equation;

$$V(y,p) = -\frac{[p\tau_T+1]}{[p\tau_q+1]}\frac{dW}{dy} \quad or \quad \frac{dV}{dy}(y,p) = -\frac{1}{A}\frac{d^2W}{dy^2} \quad (11)$$

Solving equations (7) and (8), using the boundary conditions given in equations (10) with equation (11), we have the following:

$$W(y,p) = \exp\left(\frac{sA}{2}y\right)[c_1\cosh(y\delta) + c_2\sinh(y\delta)] \quad (12)$$

$$F(Y,p) = [D_1\cosh(y\delta_1) + D_2\sinh(y\delta_1)]\exp\left(\frac{sy}{2P_r}\right) - \frac{1}{2P_r}\left[\frac{(c_1+c_2)\exp(y\delta)}{d_1} + \frac{(c_1-c_2)\exp(-y\delta)}{d_2}\right]\exp\left(\frac{sA}{2}y\right) \quad (13)$$

$$V(y,p) = -\frac{1}{A}\exp\left(\frac{sA}{2}y\right)\{\delta[c_1\sinh(y\delta) + c_2\cosh(y\delta)] + \frac{sA}{2}[c_1\cosh(y\delta) + c_2\sinh(y\delta)]\} \quad (14)$$

Where,

$$\delta = \sqrt{\left(\frac{sA}{2}\right)^2 + pA}; \quad \delta_1 = \sqrt{\left(\frac{s}{2P_r}\right)^2 + \frac{p}{P_r}}; \quad A = \frac{[p\tau_q+1]}{[p\tau_T+1]};$$

$$c_1 = \frac{1}{p}\frac{[r_t x_7 - x_5]}{[x_4x_7 - x_5x_6]}; \quad c_2 = -\frac{1}{p}\frac{[r_t x_6 - x_4]}{[x_5x_6 - x_4x_7]};$$

$$x_1 = \delta\sinh(\delta) + \frac{sA}{2}\cosh(\delta); \quad x_2 = \delta\cosh(\delta) + \frac{sA}{2}\sinh(\delta); \quad x_3 = \exp\left(\frac{sA}{2}\right);$$

$$x_4 = 1 - \frac{kn}{P_r}\frac{sA}{2}; \quad x_5 = -\frac{kn}{P_r}\delta; \quad x_6 = \left[\cosh(\delta) + \frac{\mathrm{kn}}{\mathrm{P_r}}\mathrm{x_1}\right]\mathrm{x_3}; \quad x_7 = \left[\sinh(\delta) + \frac{\mathrm{kn}}{\mathrm{P_r}}\mathrm{x_2}\right]\mathrm{x_3};$$

$$d_1 = \frac{(AP_r-1)}{P_r}\left[\frac{s^2A}{2} + p + s\delta\right]; \; d_2 = \frac{(AP_r-1)}{P_r}\left[\frac{s^2A}{2} + p - s\delta\right]; \; d_3 = \frac{1}{2P_r}\left[\frac{(c_1+c_2)\left(\delta+\frac{sA}{2}\right)}{d_1} + \frac{(c_1-c_2)\left(\frac{sA}{2}-\delta\right)}{d_2}\right];$$

$$d_4 = \frac{1}{2P_r}\exp\left(\frac{sA}{2}\right)\left[\frac{(c_1+c_2)\left(\delta+\frac{sA}{2}\right)\exp(\delta)}{d_1} + \frac{(c_1-c_2)\left(\frac{sA}{2}-\delta\right)\exp(-\delta)}{d_2}\right];$$

$$d_5 = \left[\frac{s}{P_r}\cosh(\delta_1) + \delta_1\sinh(\delta_1)\right]; \quad d_6 = \left[\frac{s}{P_r}\sinh(\delta_1) + \delta_1\cosh(\delta_1)\right];$$

$$d_7 = \frac{1}{2P_r}\left[\frac{(c_1+c_2)}{d_1} + \frac{(c_1-c_2)}{d_2}\right] - d_3\left(\frac{kn}{P_r}\right);$$

$$d_8 = \frac{1}{2P_r}\exp\left(\frac{sA}{2}\right)\left[\frac{(c_1+c_2)\exp(\delta)}{d_1} + \frac{(c_1-c_2)\exp(-\delta)}{d_2}\right];$$

$$d_9 = \cosh(\delta_1) + \frac{kn}{P_r}d_5; \quad d_{10} = \sinh(\delta_1) + \frac{kn}{P_r}d_6; \quad d_{11} = \left(d_8 + \frac{kn}{P_r}d_4\right)\exp\left(-\frac{s}{2P_r}\right);$$

$$d_{12} = 1 - s\frac{kn}{P_r^2}; \quad d_{13} = -\delta_1\frac{kn}{P_r};$$

$$D_1 = -\frac{[d_{11}d_{13} - d_7d_{10}]}{[d_{12}d_{10} - d_9d_{13}]}; \quad D_2 = \frac{[d_{11}d_{12} - d_9d_7]}{[d_{10}d_{12} - d_{13}d_9]}.$$

Equations (12) and (13) are inverted in terms of the Riemann-sum approximation ([2], [17]) as.

$$T(y,t) \cong \frac{e^{\varepsilon t}}{t}\left[\frac{1}{2}W(y,\varepsilon) + Re\sum_{k=1}^{N}W\left(y,\varepsilon + \frac{ik\pi}{t}\right)(-1)^k\right]$$

**2.1 Rate of Heat Transfer and Skin Friction.** The rate of heat transfer which is represented by the Nusselt number $(Nu)$ is obtained by differentiating eq. (9), the temperature with respect to $y$ as follows:

$$Nu = \frac{dW}{dy}|_{y=0,1} \cong \frac{e^{\varepsilon t}}{t}\left[\frac{1}{2}\frac{dW}{dy}(y,\varepsilon) + Re\sum_{k=1}^{N}\frac{dW}{dy}\left(y,\varepsilon + \frac{ik\pi}{t}\right)(-1)^k\right] \quad (15)$$

Where,

$$\frac{dW}{dy} = c_1\left[\delta sinh(\delta y) + \frac{sA}{2}cosh(\delta y)\right]\exp\left(\frac{sA}{2}y\right) + c_2\left[\delta cosh(\delta y) + \frac{sA}{2}sinh(\delta y)\right]\exp\left(\frac{sA}{2}y\right) \quad (16)$$

The rate of heat transfer at the cold porous wall is obtained by substituting $y = 0$, and at the hot wall when $y = 1$ in Eq. (16). We have,

$$Nu_0 = \frac{dW}{dy}|_{y=0} = \delta c_2 + \frac{sA}{2}c_1 \quad (17)$$

$$Nu_1 = \frac{dW}{dy}|_{y=1} = [c_1x_1 + c_2x_2]x_3 \quad (18)$$

The skin friction, $\tau u$, is defined as $\frac{dF}{dy}$, and obtained by differentiating Eq. (10) with respect to $y$ as follows:

$$\frac{dF}{dy} =$$
$$\frac{s}{2Pr}[D_1\cosh(y\delta_1) + D_2\sinh(y\delta_1)]\exp\left(\frac{s}{2Pr}y\right) +$$
$$[D_1\delta_1\sinh(y\delta_1) + D_2\delta_1\cosh(y\delta_1)]\exp\left(\frac{s}{2Pr}y\right) - \frac{1}{2Pr}\exp\left(\frac{sA}{2}y\right)\left[\frac{(c_1+c_2)\left(\delta+\frac{sA}{2}\right)\exp(\delta y)}{d_1} + \frac{(c_1-c_2)\left(\frac{sA}{2}-\delta\right)\exp(-\delta y)}{d_2}\right] \quad (19)$$

Where,

$$\tau_0 = \frac{dF}{dy}|_{y=0} = \frac{s}{2Pr}D_1 + \delta_1 D_2 - d_3 \quad (20)$$

$$\tau_1 = \frac{dF}{dy}|_{y=1} = d_5 exp\left(\frac{s}{2Pr}\right)D_1 + d_6 exp\left(\frac{s}{2Pr}\right)D_2 - d_4 \quad (21)$$

This equation represent the skin friction at both walls of the micro-channel and is given by the Riemann-sun for Laplace inversion as;

$$\tau_{0,1} = \frac{dF}{dy}|_{y=0,1} \cong \frac{e^{\varepsilon t}}{t}\left[\frac{1}{2}\frac{dF}{dy}(y,\varepsilon) + Re\sum_{n=1}^{N}\frac{dF}{dy}\left(y,\varepsilon+\frac{in\pi}{t}\right)(-1)^n\right]_{y=0,1}$$

**2.2 Steady State.** The expressions for the steady state velocity distribution, $U_{ss}$, and that of the temperature distribution, $T_{ss}$, are obtained by setting $\frac{\partial u}{\partial t}$ in Eq. (3), and $\frac{\partial T}{\partial t}$ in Eq. (4) equal to zero. We then obtain the following ordinary differential equations:

$$\frac{d^2U_{ss}}{dy^2} - \frac{s}{Pr}\frac{dU_{ss}}{dy} = -T_{ss} \quad (22)$$

$$\frac{d^2T_{ss}}{dy^2} - s\frac{dT_{ss}}{dy} = 0 \quad (23)$$

The solutions of Eqs. (22) and (23) together using the boundary conditions in Eq. (6a) to (6e) are:

$$T_{ss}(y) = A + B\exp(sy) \quad (24)$$

$$U_{ss}(y) = A\left[\frac{y}{s} + \frac{Pr}{s^2}\right] - \frac{B}{s(Pr-1)}\exp(sy) - \frac{Pr}{s}k_1 + k_2\exp\left(\frac{sy}{Pr}\right) \quad (25)$$

Where,

$$B_1 = 1 - \frac{kn}{Pr}s\,; \quad B_2 = \exp(s)\left[1 + \frac{kn}{Pr}s\right];$$
$$A = \frac{(1-r_t)}{(B_2-B_1)}; \quad B = \frac{r_tB_2-B_1}{B_2-B_1}.$$
$$B_3 = A\left[\frac{Pr}{s^2} - \frac{kn}{Pr}.\frac{1}{s}\right] + B\left[\frac{kn}{Pr}.\frac{1}{(Pr-1)} - \frac{1}{s(Pr-1)}\right];\ B_4 = \left[\frac{kn}{Pr}.\frac{s}{Pr} - 1\right];\ B_5 = \frac{Pr}{s};$$
$$B_6 = -\left[1 - \frac{kn}{Pr}.\frac{s}{Pr}\right]\exp\left(\frac{s}{Pr}\right);\ B_7 = k_1B_5 + k_2B_6;$$
$$k_1 = -\frac{B_4B_7-B_3B_6}{B_5B_6-B_4B_5};\ k_2 = \frac{B_5B_7-B_3B_5}{B_5B_6-B_4B_5}.$$

The numerical values of the temperature and velocity obtained exactly for the steady state (by equations (23) and (24)) are compared with those of the transient state obtained using the Riemann-sum approximation method in Table 1. These values are generated when $s = 0.05$, $r_t = 0.5$, $kn = 0.01$, $Pr = 0.71$ and $\tau_q = 0.01$, $\tau_T = 0.001$. We observed in Table 1 that at a particular point in the channel, the transient temperature increases with time until it attains its steady state. The transient state temperature values when $t = 1.0$ are observed to coincide with the steady state temperature values. We can conveniently conclude that there is an impeccable agreement between the Riemann-sum approximation method and the analytical method. Similarly, the numerical values of the velocity obtained analytically for steady state are also compared with those of the transient state obtained using the Riemann-sum approximation method in Table 2. The values are generated when $s = 0.05$, $r_t = 0.5$, $kn = 0.01$, $Pr = 0.71$, $\tau_T = 0.01$ and $\tau_q = 0.001$. The transient velocity also increases with time until it attains approximately the steady state about when $t = 1.0$ as shown in table 2.

**Table 1. Comparison of the numerical values of the transient state temperature obtained using the Riemann-sum approximation method and the steady state temperature obtained analytically when $s = 0.05$, $Pr = 0.71$, $r_t = 0.5$, $kn = 0.01$, $\tau_T = 0.001$ $and$ $\tau_q = 0.01$.**

| $t$ | $y$ | Transient state temp. | Steady state temp. |
|---|---|---|---|
| 0.4 | 0.2 | 0.5916 | 0.6020 |
| | 0.4 | 0.6820 | 0.6983 |
| | 0.6 | 0.7791 | 0.7955 |
| | 0.8 | 0.8829 | 0.8938 |
| 0.6 | 0.2 | 0.6007 | 0.6020 |
| | 0.4 | 0.6963 | 0.6983 |
| | 0.6 | 0.7935 | 0.7955 |
| | 0.8 | 0.8925 | 0.8938 |
| 0.8 | 0.2 | 0.6019 | 0.6020 |
| | 0.4 | 0.6981 | 0.6983 |
| | 0.6 | 0.7953 | 0.7955 |
| | 0.8 | 0.8938 | 0.8938 |
| 1.0 | 0.2 | 0.6020 | 0.6020 |
| | 0.4 | 0.6983 | 0.6983 |
| | 0.6 | 0.7956 | 0.7955 |
| | 0.8 | 0.8938 | 0.8938 |

**Table 2. Comparison of the numerical values of the transient state velocity obtained using the Riemann-sum approximation method and the steady state velocity obtained analytically when $s = 0.05$, $Pr = 0.71$, $r_t = 0.5$, $kn = 0.01$, $and$ $\tau_T = 0.01$, $\tau_q = 0.001$.**

| $t$ | $y$ | Transient state velocity. | Steady state velocity. |
|---|---|---|---|
| 0.4 | 0.2 | 0.0687 | 0.0850 |
| | 0.4 | 0.1047 | 0.1304 |
| | 0.6 | 0.1110 | 0.1368 |
| | 0.8 | 0.0818 | 0.0983 |
| 0.6 | 0.2 | 0.0800 | 0.0850 |
| | 0.4 | 0.1226 | 0.1304 |
| | 0.6 | 0.1291 | 0.1368 |
| | 0.8 | 0.0936 | 0.0983 |
| 0.8 | 0.2 | 0.0837 | 0.0850 |
| | 0.4 | 0.1284 | 0.1304 |
| | 0.6 | 0.1350 | 0.1368 |
| | 0.8 | 0.0975 | 0.0983 |
| 1.0 | 0.2 | 0.0848 | 0.0850 |
| | 0.4 | 0.1302 | 0.1304 |
| | 0.6 | 0.1369 | 0.1368 |
| | 0.8 | 0.0983 | 0.0983 |

## 3. RESULTS AND DISCUSSION

The basic parameters that govern the transient flow of the system under consideration include: the Knudsen number $(kn)$ which gives the mean free path length of the fluid molecules, the phase lags $(\tau_q)$ and $(\tau_T)$ which respectively give, the duration of free time during which the heat flux vector due to phonon collision and phase-lag in temperature gradient increase; and suction/injection parameter $(s)$ which were simultaneously applied at the opposite walls of the micro-channel. Line graphs displaying the transient hydrodynamics and thermal behaviour of the fluid flow are presented. These figures reveal the observable effects of suction/injection, as well as the influences of the other governing parameters on the flow characteristics.

Figures 2a and 2b show the spatial temperature distribution for varying values of $kn$ within the rarefaction regime. We observe that when suction is introduced at the cold wall, increase in $kn$ increases the fluid temperature near the wall while injection at the cold wall causes decrease in the temperature as $kn$ increases.

The spatial temperature distributions for different values of $\tau_T$ are given by figures 3a and 3b. In both cases of suction and injection at cold wall, the temperature increases with increase in $\tau_T$. However, injection appears to increase slightly the temperature than suction.

Figures 4a and 4b show the cases where $\tau_q$ varies in the channel. Increase in $\tau_q$ decreases the thermal behaviour in the micro-channel. This is in contrast with thermal behaviour observed in figures 3a and 3b.

The role of suction/injection on the temperature profile in the micro-channel is given in figure 5a when $\tau_q < \tau_T$ and in figure 5b when $\tau_q > \tau_T$. Suction imposed at the cold wall gives higher temperature compared to injection at the wall. We also observe that increase in suction/injection decreases the spatial temperature of the fluid.

Figures 6a and 6b present the transient temperature profile at different times when suction and injection are applied at the cold wall. It is obvious that the as time increases the temperature increases and subsequently

approaches steady state. Also, as time increases the temperature jump decreases at the walls. The temperature jump is observed to be more significant at the cold wall with suction than injection.

The effect of suction/injection s on the velocity profile when $\tau_q > \tau_T$, $\tau_q < \tau_T$, and for higher value of $\tau_T$ are respectively given in figures 7a, 7b, and 7c. We observe in figure 7a that increase in s at any given time increases the velocity of the fluid. Subsequently, increase in suction decreases the velocity slip of the fluid at the hot wall. Hence, we conclude that for $\tau_q > \tau_T$ (i.e. when the heat flow is motivated by the temperature gradient vector), suction at the cold wall influences the velocity profile. Whereas, for $\tau_T > \tau_q$, (i.e. when the heat flux vector is the cause of heat flow [6, 7]), the increase in suction increases the velocity slip at the hot wall. However, the spatial velocity distribution increases with decrease in s. Also, at higher value of $\tau_T$, (as in fig. 7c), it is obvious that the velocity slip at the hot wall is higher in comparison to that observed in fig. 7b and there is the presence of velocity slip at the cold wall which increases as s increases.

Transient velocity profile for different values of time in the absence suction/injection are given by figures 8a and 8b respectively for $\tau_q > \tau_T$ and $\tau_T > \tau_q$. Nevertheless, the fluid velocity increases significantly with increase in time near the hot wall in both cases. We observe that when $\tau_T > \tau_q$, the fluid velocity is higher compared with when $\tau_q > \tau_T$. We therefore conclude that when the temperature gradient vector present is the cause for the heat flow, the velocity distribution in the channel is higher than when the heat flux vector is the motivator of the heat flow.

Figures 9a and 9b describe the transient temperature difference at both walls respectively as suction/injection s varies with the Knudsen number $Kn$ while other parameters are fixed. From these figures, we can deduce that as s increases the temperature difference decreases at both cold and hot walls. However, as $Kn$ increases, the temperature difference increases at the cold wall but decreases rapidly at the hot wall.

Furthermore, the effects of varying suction/injection with time and the role of the dual phase lags $\tau_q$ and $\tau_T$ on the temperature difference at the walls are given by figs. 10a and 10b at the cold wall, and figs. 10c and 10d at the hot wall. In general, the temperature difference increases as s decreases as observed above in figs. 9a and 9b. It is interesting to note that at both walls, the temperature differences are higher when $\tau_T > \tau_q$ in comparison with when $\tau_q > \tau_T$.

In figures 11a and 11b we describe the velocity difference at the hot wall as $\tau_T$ is allowed to vary with $Kn$. Clearly, increase in $Kn$ increases the velocity difference for all values of $\tau_T$ when suction and injection are imposed at the cold wall. It is interesting to note that with suction at the cold wall an upward surge (brief shock) in the velocity difference is noticed at $\tau_T = 0.6$, while sharp drop (brief shock) in the velocity difference is noted at this value when injection is imposed at the cold wall. This can be attributed with the phase lag in the temperature gradient vector due to phonon collision during heat flux, which builds up energy with injection but expends energy with suction. As a result, higher fluid buoyancy is present with injection resulting to a higher velocity difference after a brief drop (as in fig. 11b), while the reverse case is noted with suction in figure 11a.

Figures 12a and 12b illustrate the velocity difference at the hot wall as $\tau_T$ varies with time. As $\tau_T$ increases the velocity difference increases which becomes insignificant at higher values of $\tau_T$; especially with the presence suction (fig. 12a). But with injection at the cold wall, increase in $\tau_T$ decreases the velocity difference as time proceeds (fig. 12b).

The role of suction/injection on the walls velocity differences are presented by figures 13a and 13b at the cold wall; and by figures 13c and 13d at the hot wall as $Kn$ varies. It is clear that at the cold wall the transient velocity difference increases as s increases also as $Kn$ increases. Higher wall velocity difference is observed when $\tau_T > \tau_q$ than when $\tau_q > \tau_T$ at the cold wall. However, at the hot wall (figs. 13c and 13d), increase in s decreases the velocity difference as $Kn$ increases. It is also obvious that as $\tau_T > \tau_q$ the velocity difference is higher in comparison with the case where $\tau_q > \tau_T$ (fig. 13c).

The variation of the Nusselt number (Nu) with suction/injection s in the DPL micro-channel transient fluid flow are presented in figures 14a and 14b at the cold wall; while figures 14c and 14d describe the variation of Nu at the hot wall as $Kn$ varies. The increase in s decreases Nu at the cold wall of the micro-channel when $\tau_T > \tau_q$ while increase in s increases Nu at the cold wall when $\tau_q > \tau_T$. At the hot wall, the Nusselt number increases as s increases across the micro-channel. However, higher Nu is observed at the hot wall when $\tau_q > \tau_T$ (fig. 14d) than when $\tau_T > \tau_q$ especially in the presence of injection.

The wall skin friction of the unsteady free convection micro-channel fluid flow, described by dual-phase-lag are given in figures 15a, 15b and 15c, in the presence of suction/injection. At the cold wall (figs. 15a and 15b), the skin friction is observed to increase as s increases. Also, when $\tau_q > \tau_T$ the skin friction is higher than when we set $\tau_T > \tau_q$. While at the hot wall, the skin friction increases with decrease in s (as in fig. 15c).

Finally, we observe from the three figures that the skin friction decreases with increase in the Knudsen number irrespective of the variation of the dual phase lag.

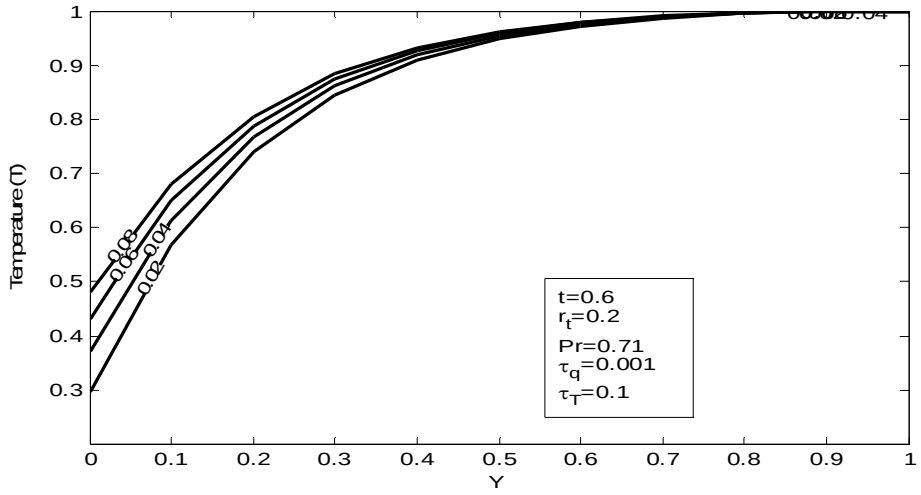


Fig.2a. Spatial temperature distribution at different Kn,when s=-5.0.

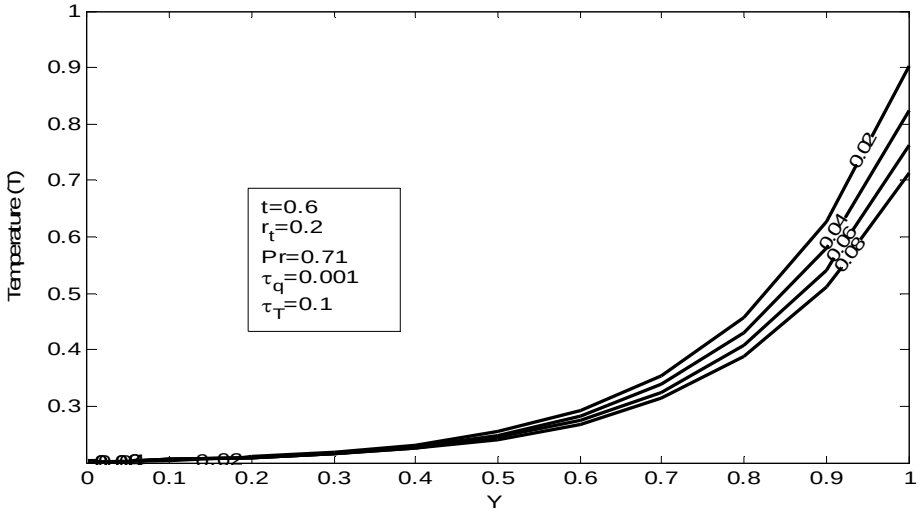


Fig.2b. Spatial temperature distribution at different Kn,when s=5.0

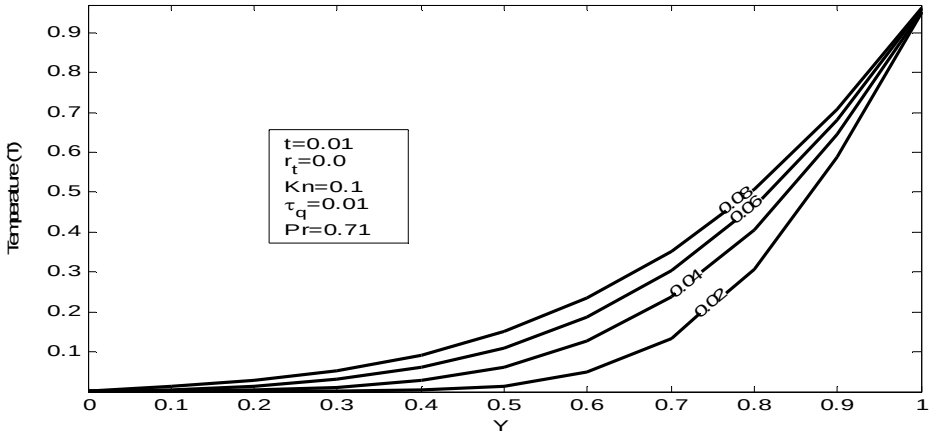


Fig.3a. Spatial temperature distribution at different $\tau_T$ when s=-5.0

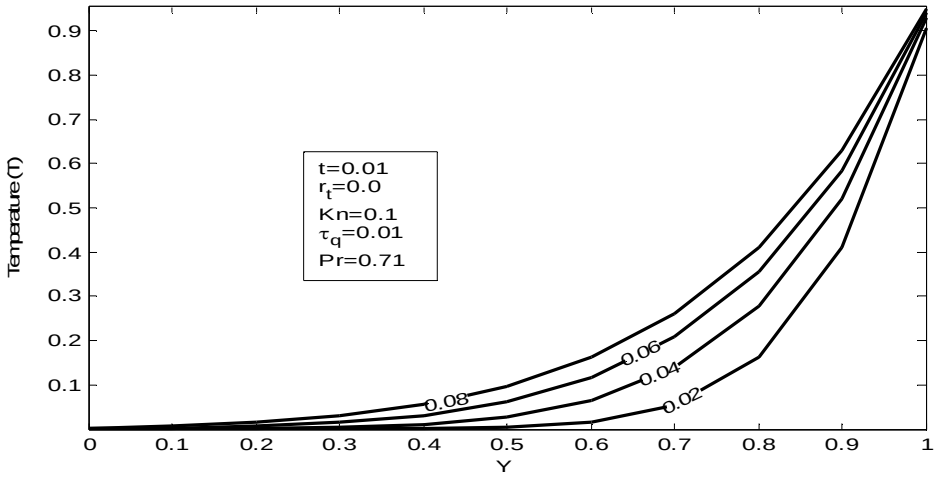


Fig.3b. Spatial temperature distribution at different $\tau_T$ when s=5.0

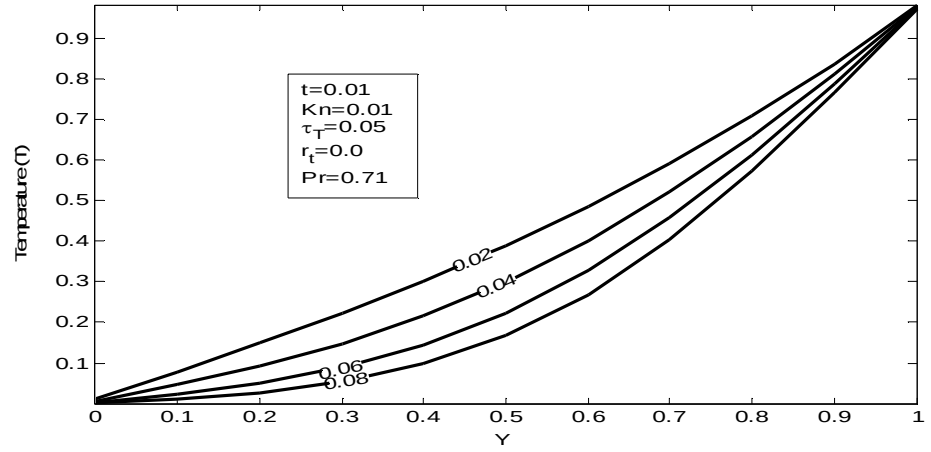


Fig.4a. Spatial temperature distribution at different $\tau_q$ when s=-5.0

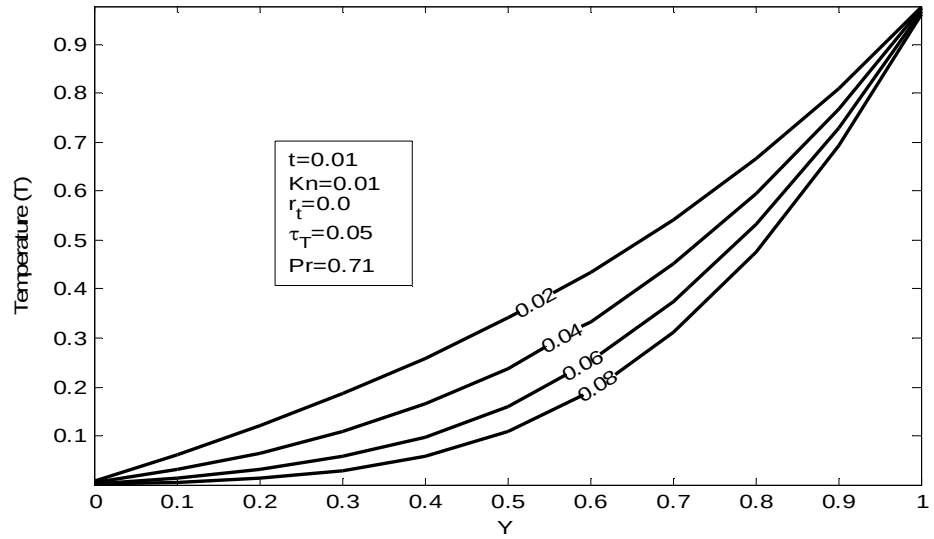


Fig.4b. Spatial temperature distribution at different $\tau_q$ when s=5.0

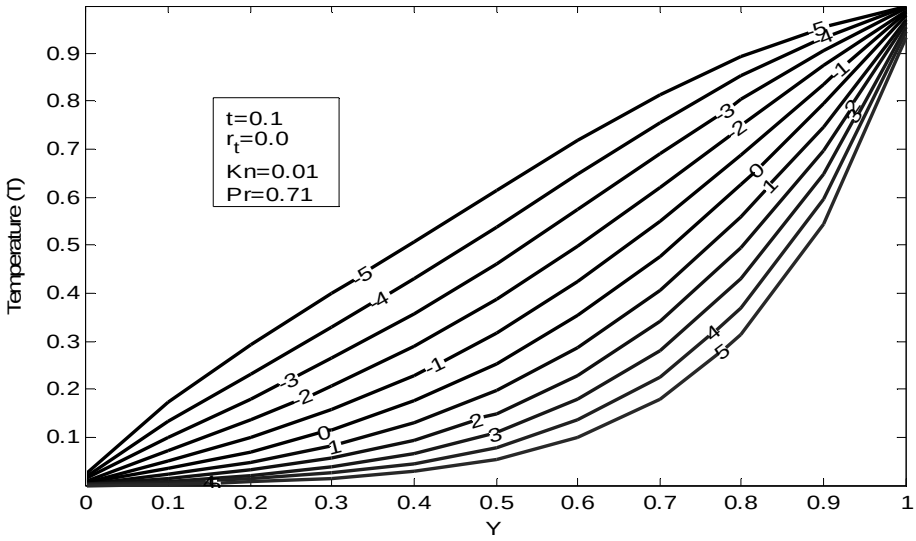


Fig.5a. Effect of S on the temperature profile when $\tau_T$=0.01, $\tau_q$=0.001,Kn=0.01.

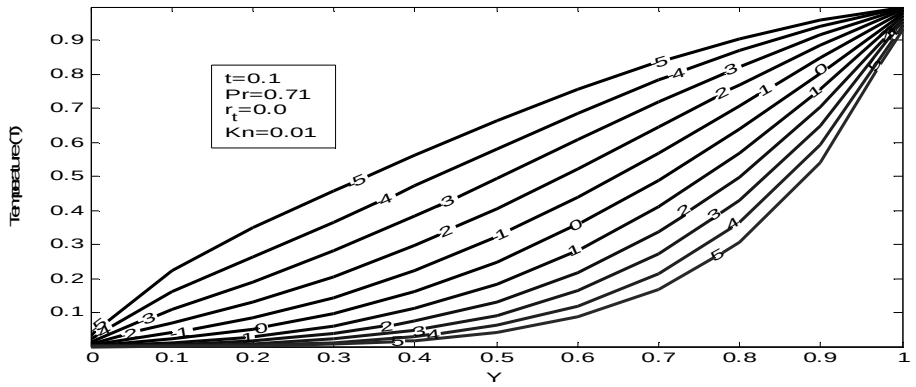


Fig.5b. Effect of S on temperature profile when t=0.1,$\tau_T$=0.001, $\tau_q$=0.01.

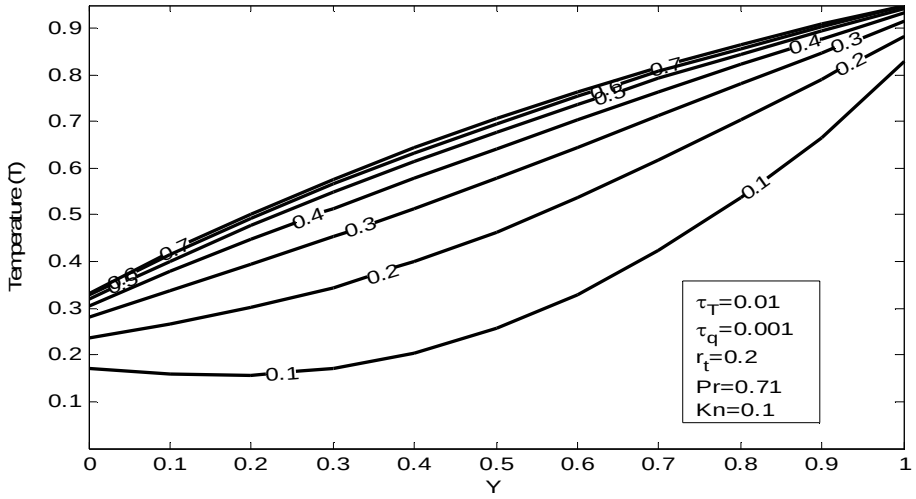


Fig.6a. Transient temperature profile for different time when s=-1.0

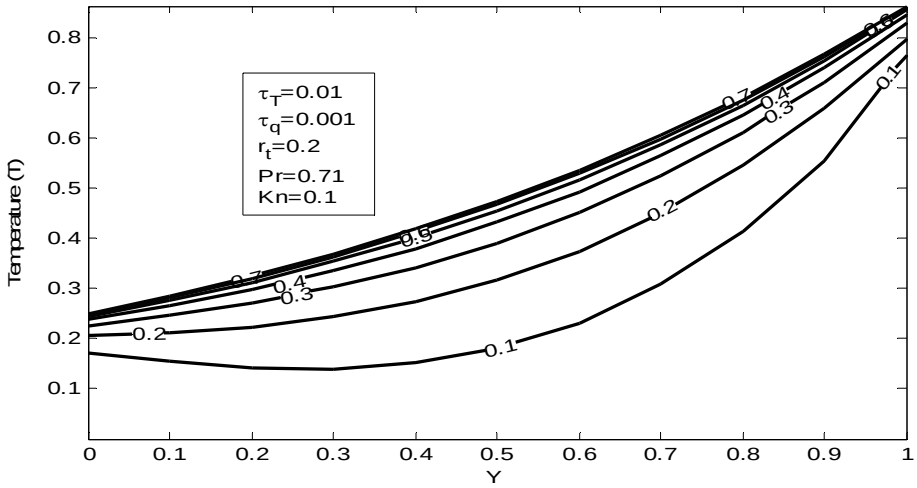


Fig.6b. Transient temperature profile for different time when s=1.0

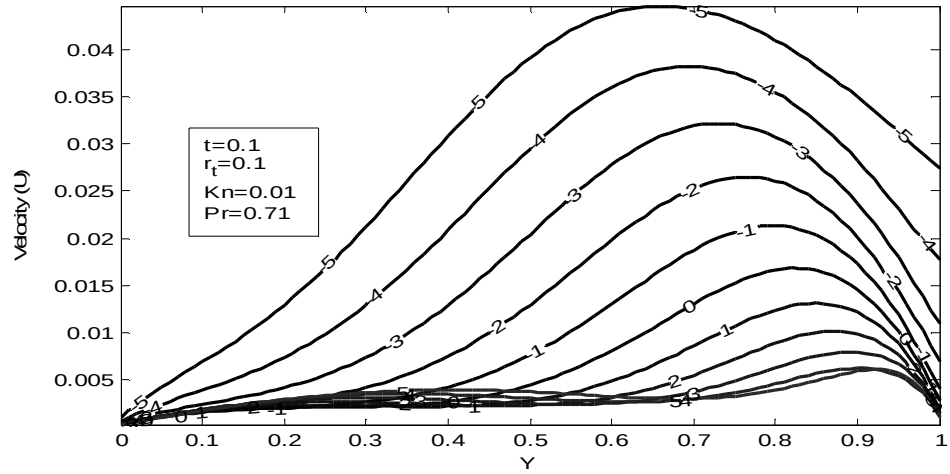


Fig.7a. Effect of S on the transient velocity when $\tau_q$=0.1 and $\tau_T$=0.01

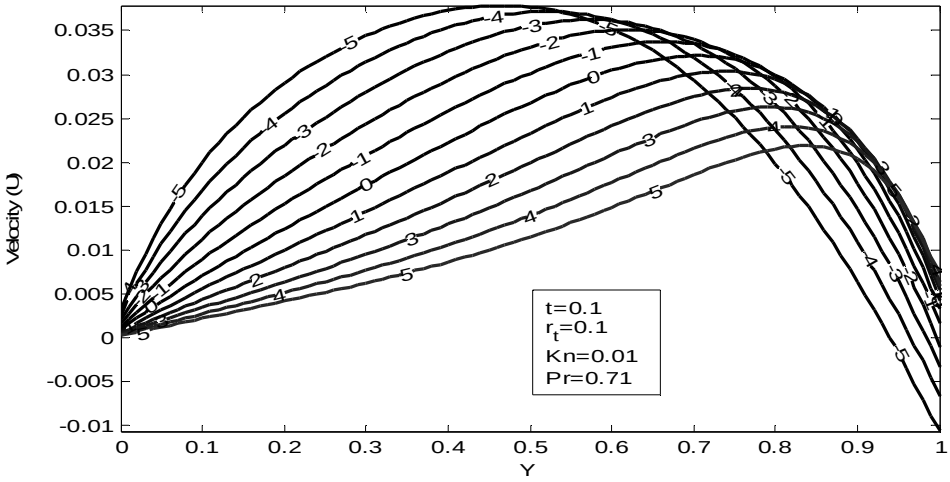


Fig.7b. Effect of S on the transient velocity when $\tau_q$=0.01 and $\tau_T$=0.1

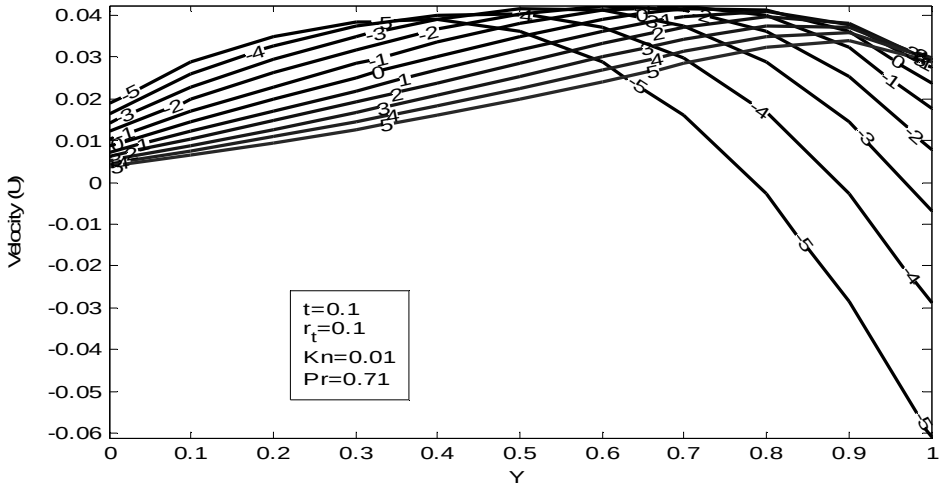


Fig.7c. Effect of S on the Transient velocity when $\tau_q$=1.0 and $\tau_T$=5.0

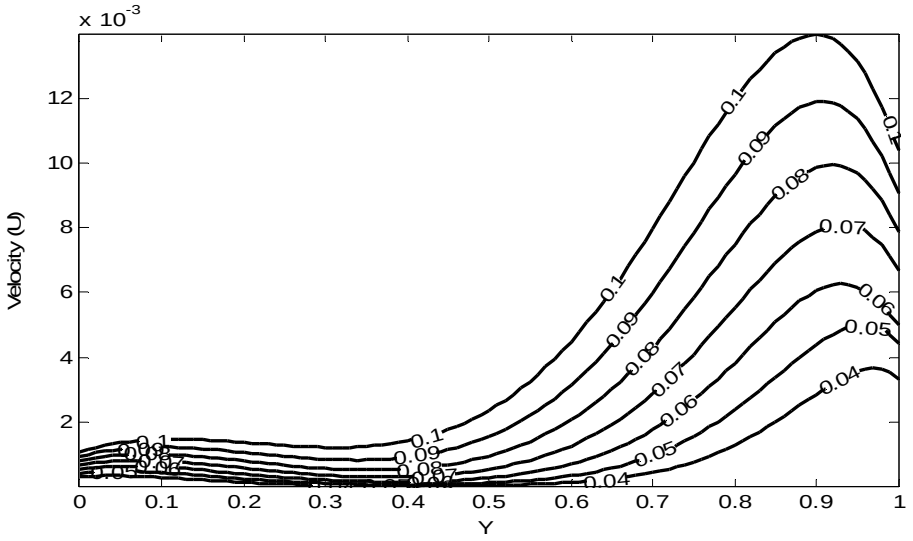


Fig.8a.Transient velocity profile when $\tau_q$=0.1,$\tau_T$=0.01, s=0.0, $r_t$=0.1, Kn=0.1, Pr=0.71

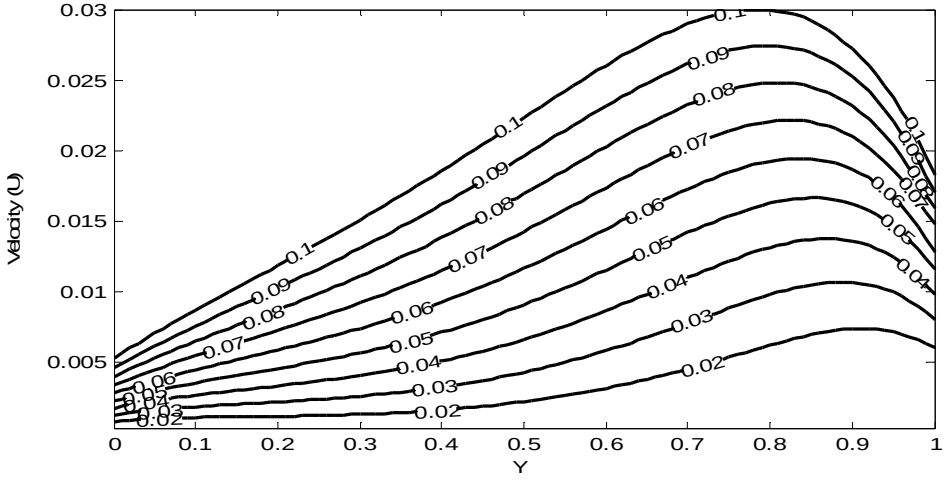


Fig.8b.Transient velocity profile when $\tau_q$=0.01,$\tau_T$=0.1, s=0.0, $r_t$=0.1, Kn=0.1, Pr=0.71

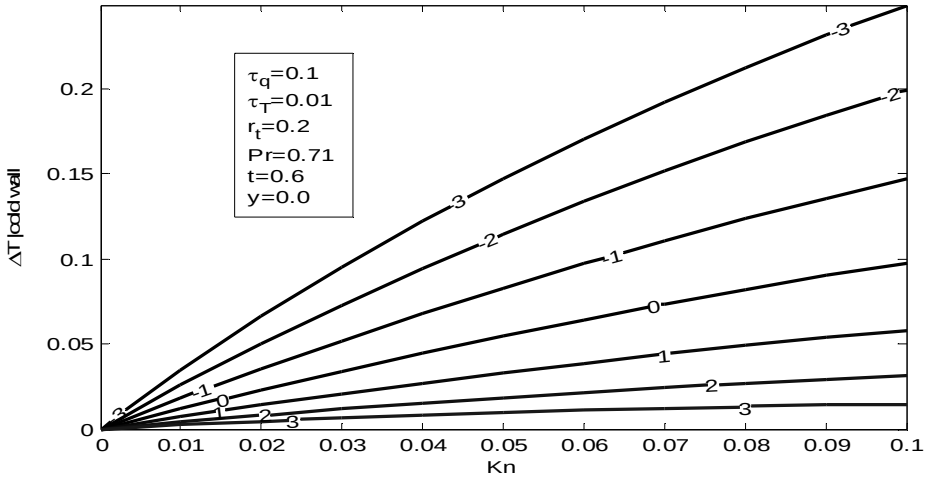


Fig.9a. The transient temperature difference at the cold wall as kn varies with s

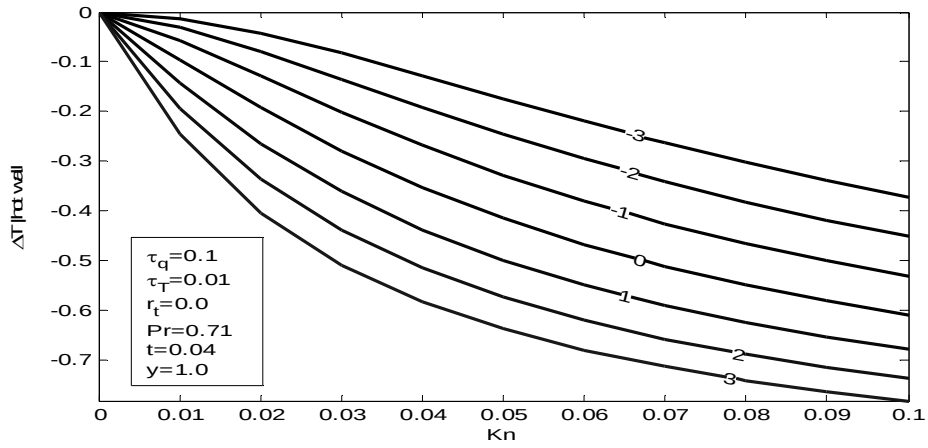


Fig.9b. The transient temperature difference at the hot wall as kn varies with s.

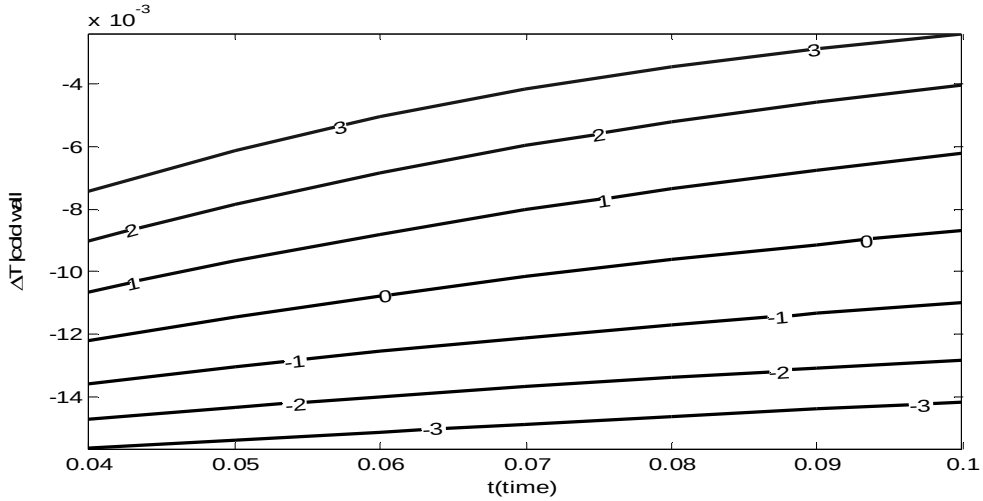


Fig.10a. The temperature difference at y=0 as time varies with s when $\tau_T$=0.1,$\tau_q$=1.0,$r_t$=0.2,kn=0.1

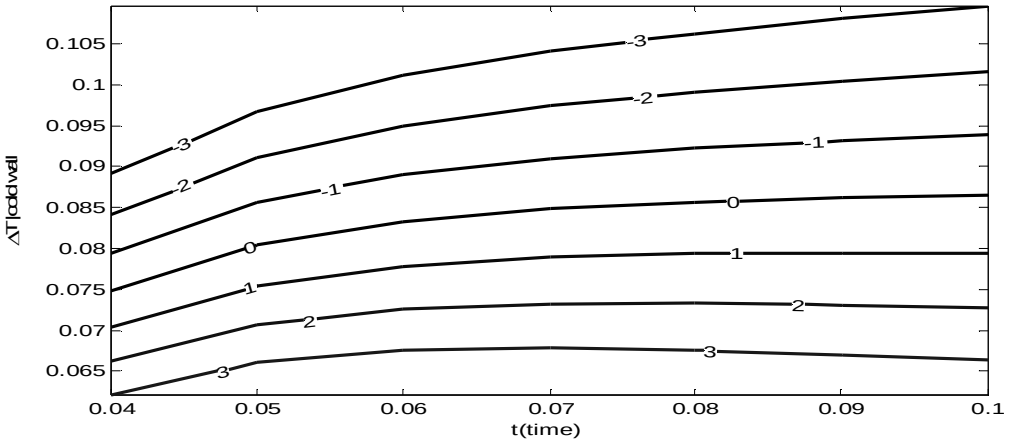


Fig.10b. The temperature difference at y=0 as time varies with s when $\tau_T$=1.0,$\tau_q$=0.1,$r_t$=0.2,kn=0.1

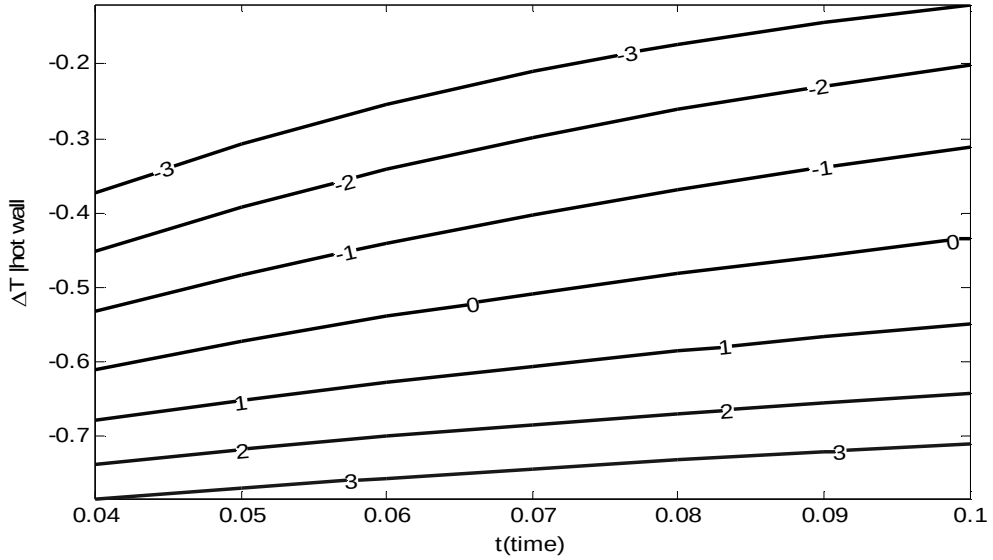


Fig.10c. The temperature difference at y=1.0 as time varies with s when $\tau_T$=0.1,$\tau_q$=1.0,$r_t$=0.0,kn=0.1

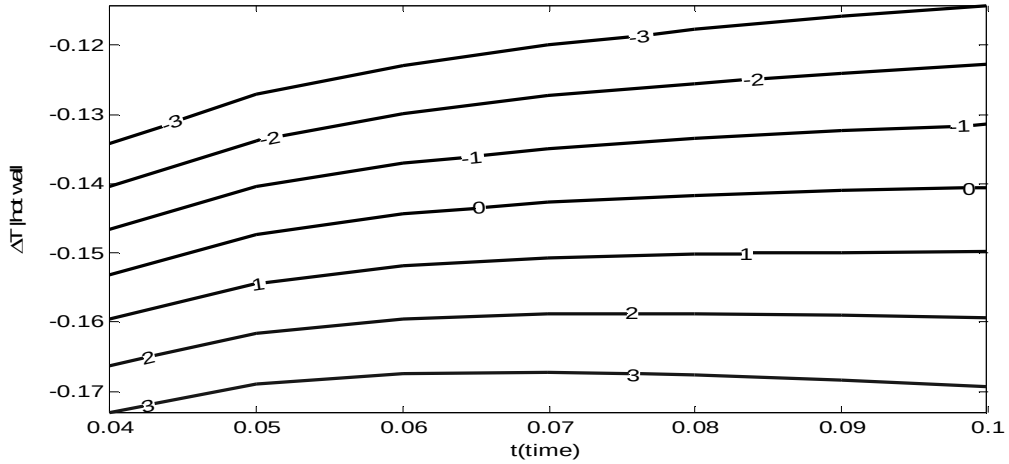


Fig.10d. The temperature difference at y=1.0 as time varies with s when $\tau_T$=1.0,$\tau_q$=0.1,$r_t$=0.0,kn=0.1

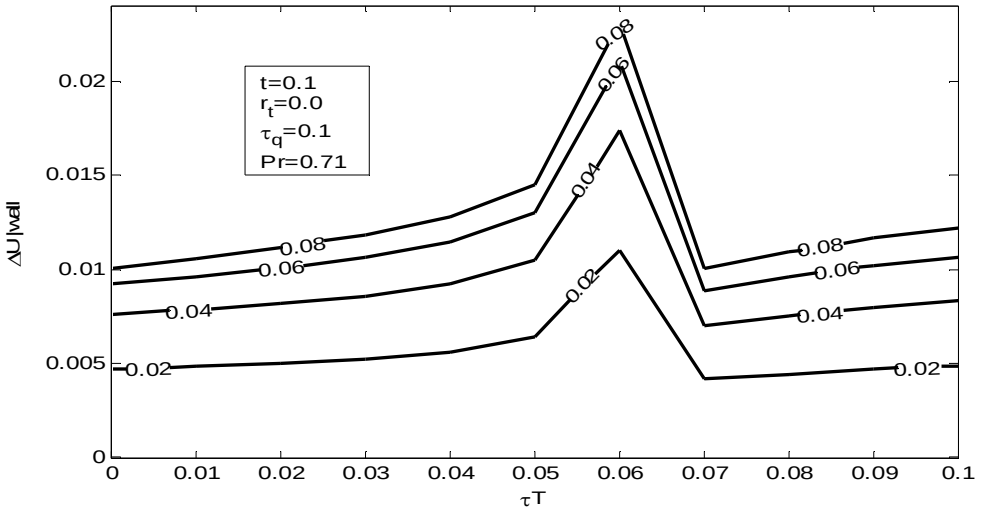


Fig.11a. Effect of $\tau_T$ on the velocity difference at y=1 with varying kn when s=-0.1

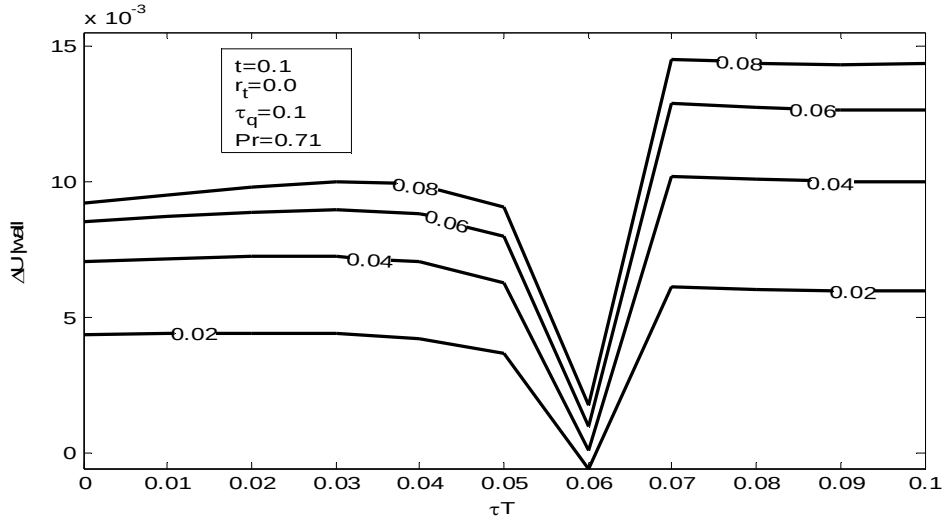


Fig.11b. Effect of $\tau_T$ on the velocity difference at y=1.0 with varying kn when s=0.1

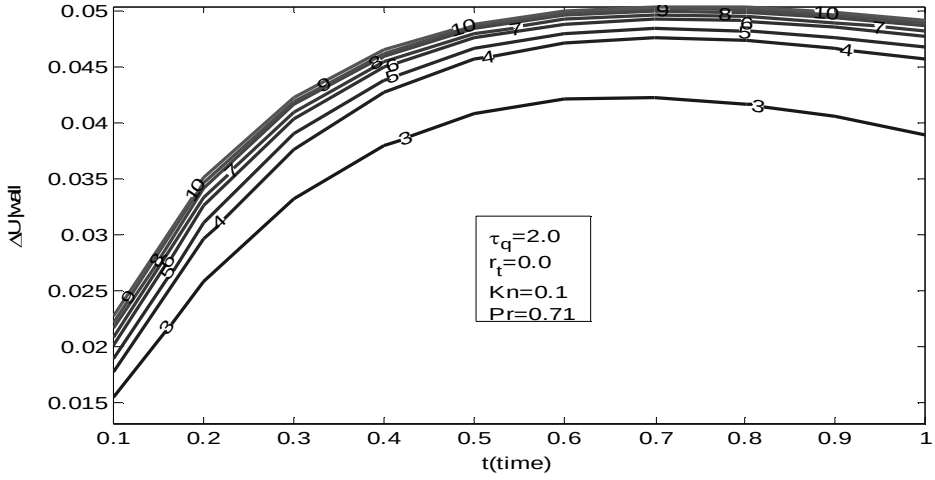


Fig.12a. Effect of $\tau_T$ on the transient velocity difference at the wall y=1.0 when s=-0.1

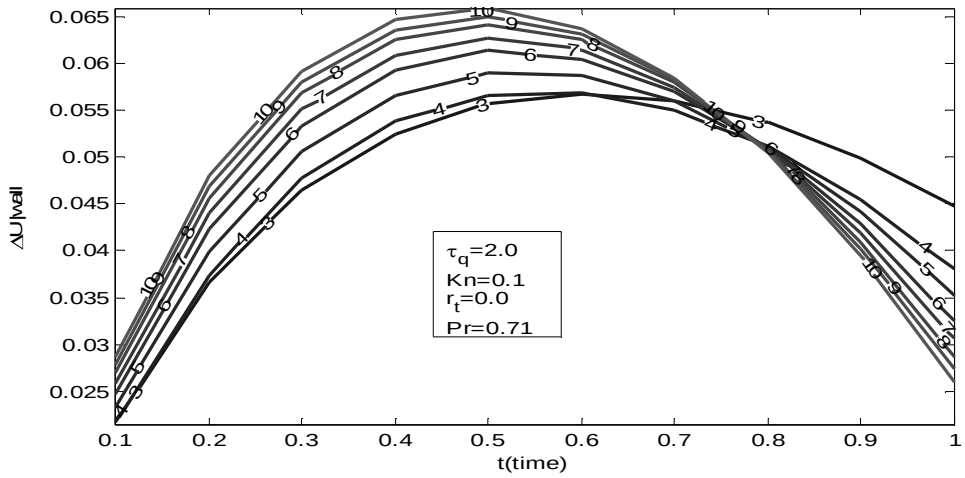


Fig.12b. Effect of $\tau_T$ on the transient velocity difference at y=1.0 when s=3.0

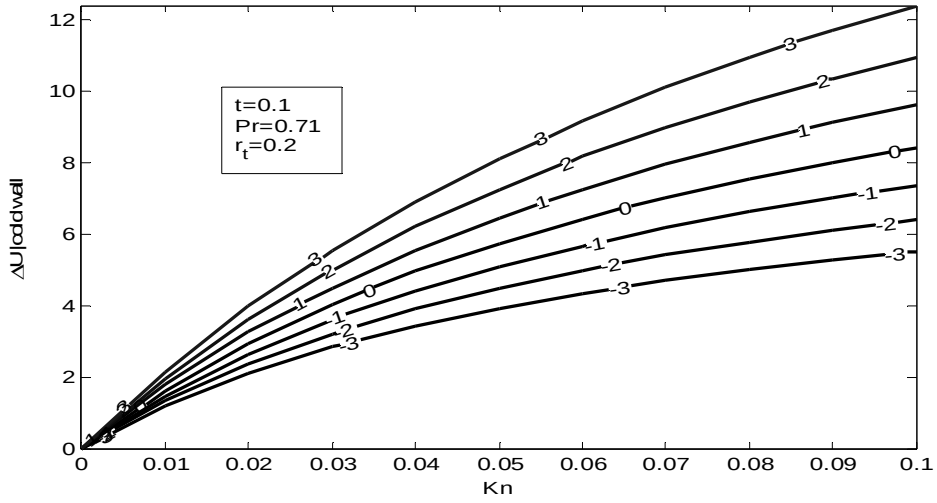


Fig.13a. Effect of S on the transient velocity difference at y=0.0 when $\tau_q$=0.01, $\tau_T$=0.001

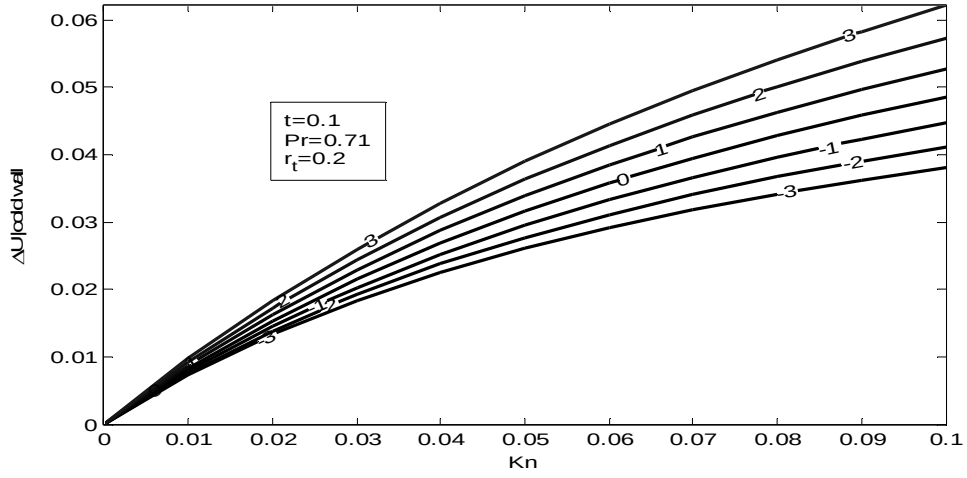


Fig.13b. Effect of S on the transient velocity difference at y=0.0 when $\tau_q$=0.001, $\tau_T$=0.01

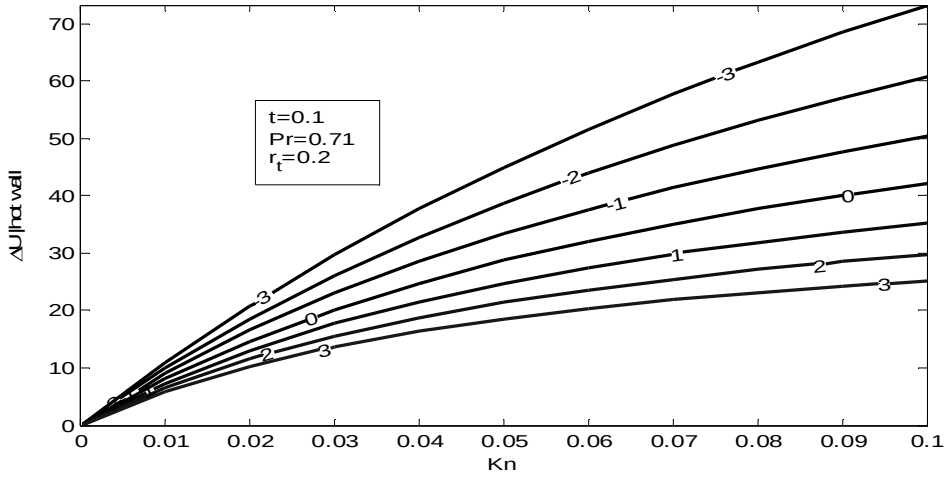


Fig.13c. Effect of S on the transient velocity difference at y=1.0 when $\tau_q$=0.01, $\tau_T$=0.001

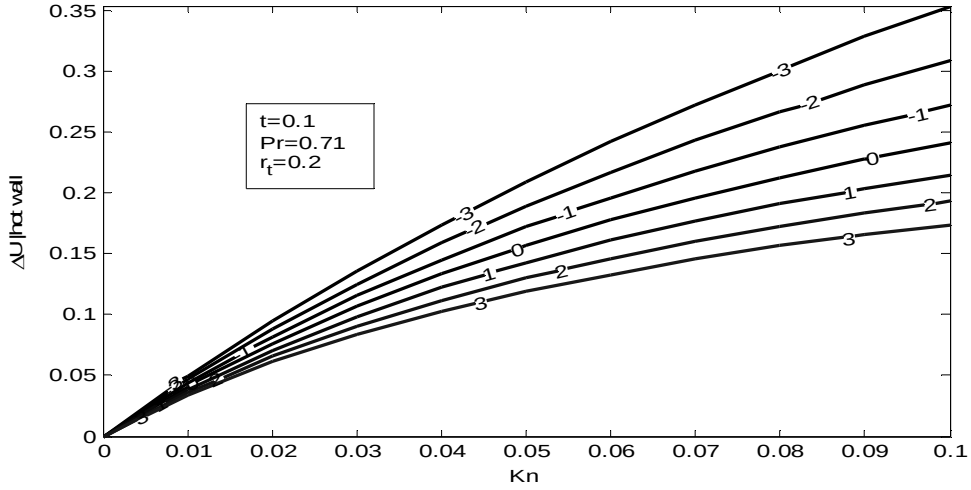


Fig.13d. Effect of S on the transient velocity difference at y=1.0 when $\tau_q$=0.001, $\tau_T$=0.01

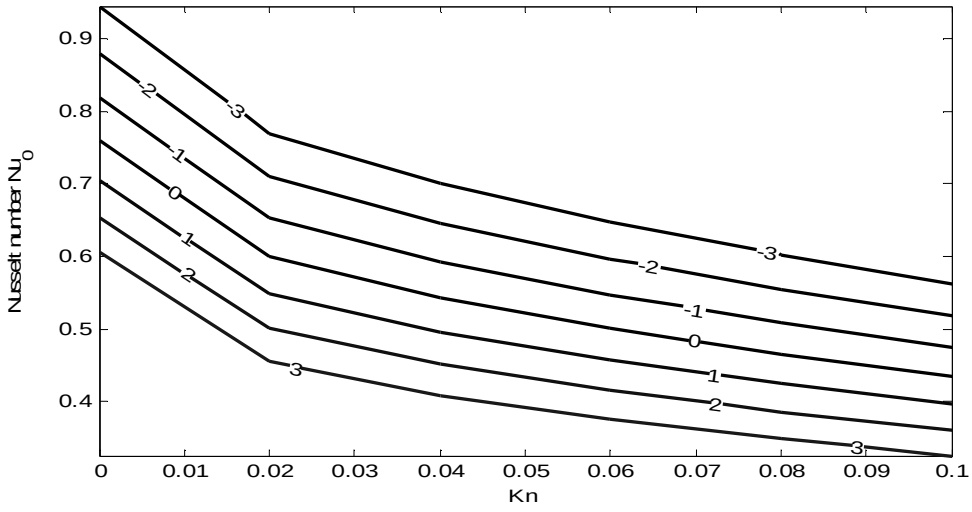


Fig.14a. Effect of S on Nu with different kn at y=0 when $\tau_q$=0.1, $\tau_T$=1.0, t=0.1, $r_t$=0.2,Pr=0.71

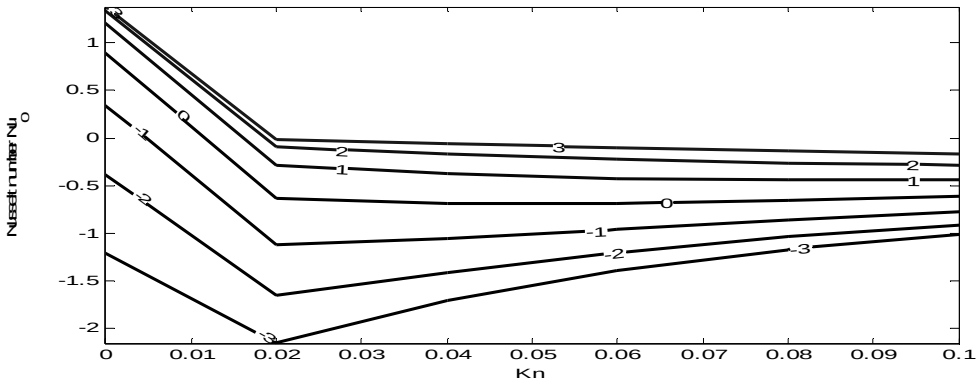


Fig.14b. Effect of S on Nu with different kn at y=0 when $\tau_q$=1.0, $\tau_T$=0.1, t=0.1, $r_t$=0.2,Pr=0.71

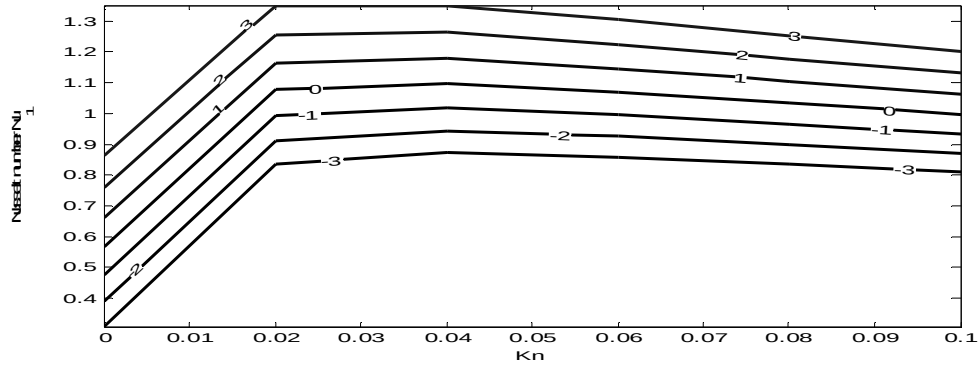


Fig.14c. Effect of S on Nu with different kn at y=1.0 when $\tau_q$=0.1, $\tau_T$=1.0, t=0.1, $r_t$=0.0,Pr=0.71

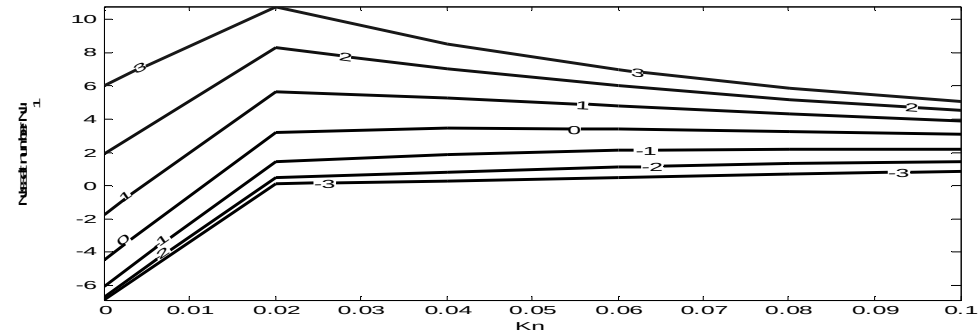


Fig.14d. Effect of S on Nu with different kn at y=1.0 when $\tau_q$=1.0, $\tau_T$=0.1, t=0.1, $r_t$=0.0,Pr=0.71

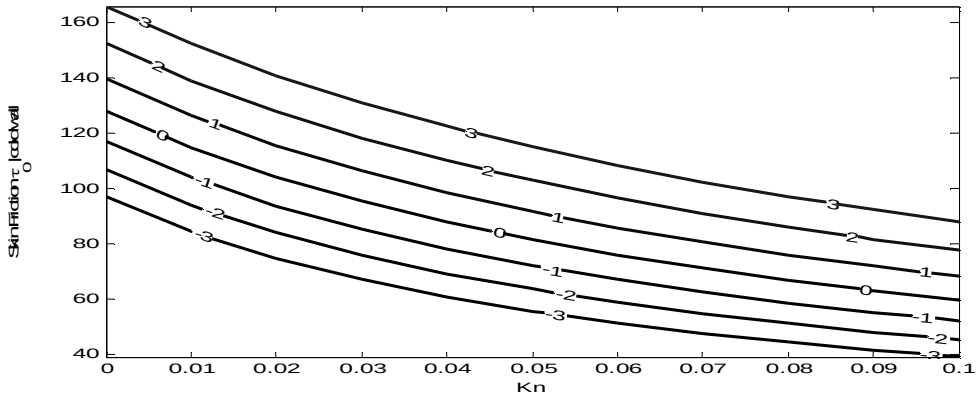


Fig.15a. Effect of S on the transient Skin friction with Kn when $\tau_q$=0.01, $\tau_T$=0.001, t=0.1, $r_t$=0.2

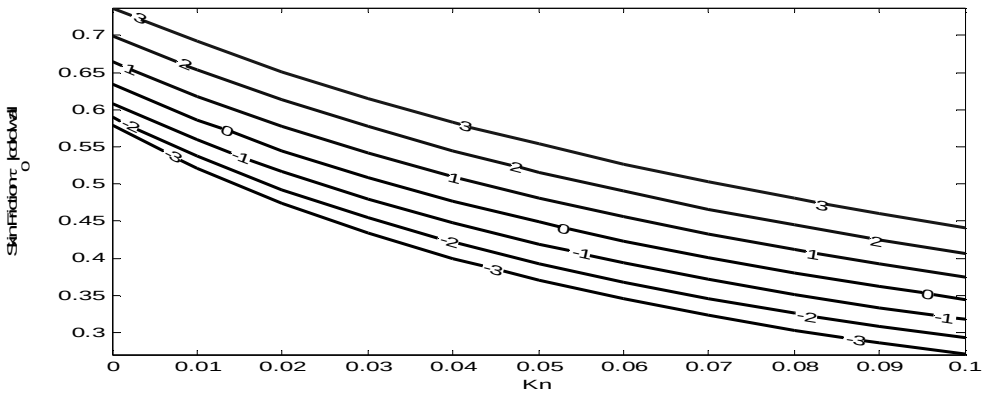


Fig.15b. Effect of S on the transient Skin friction with Kn when $\tau_q$=0.001, $\tau_T$=0.01, t=0.1, $r_t$=0.2

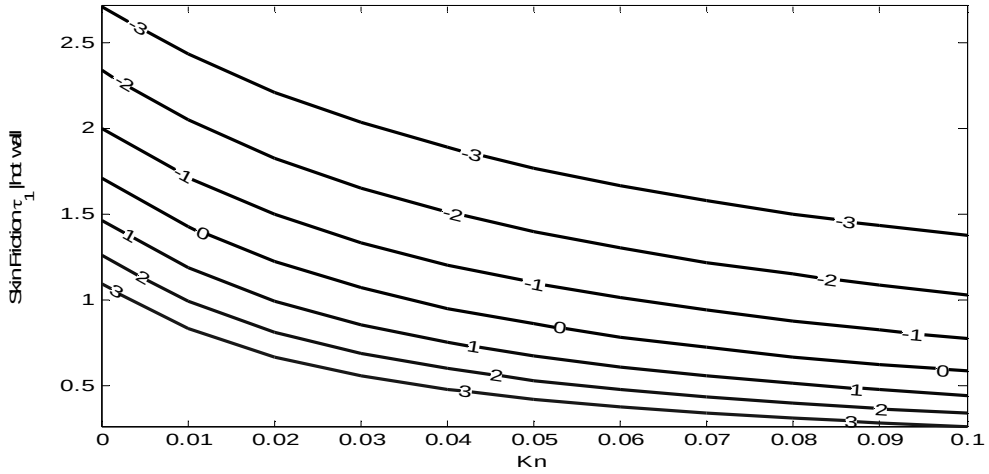


Fig.15c. Effect of S on the transient Skin friction with Kn when $\tau_q$=0.01, $\tau_T$=0.001, t=0.1, $r_t$=0.2

## 4. CONCLUSION

The present study investigated the micro-channel transient thermal and hydrodynamic behaviour under the effect of dual-phase-lag heat-conduction model with suction/injection at the porous boundary walls. The perturbations in the micro-channel unsteady thermal characteristics due to the suction/injection at the porous walls, phase-lag in heat flux $\tau_q$, the phase-lag in temperature gradient $\tau_T$ and the Knudsen number are investigated by understudying their roles on the skin friction and heat transfer at the channel walls. We observed that suction at the cold wall decreases the velocity slip at the hot wall when $\tau_q > \tau_T$ but increases wall velocity slip when $\tau_T > \tau_q$. Also, the transient Temperature and velocity profiles in the micro-channel are higher when $\tau_T > \tau_q$ than when $\tau_q > \tau_T$. The wall temperature difference increases as suction/injection decreases and the increase in $Kn$ increases the temperature difference at the cold wall but decreases at the hot wall. We also observed that as suction/injection increases, the Nusselt number increases when $\tau_T > \tau_q$ at the hot wall but increases at the cold wall when $\tau_q > \tau_T$. Finally, the wall skin friction is observed to increase at cold wall and decrease at the hot wall as suction/injection increases.

**NOMENCLATURE**

$F$ Laplace transformation of dimensionless velocity

$kn$ Knudsen number, $\lambda/L$

$r_t$ $\frac{T_{w2}-T_0}{T_{w1}-T_{w2}}$.

$T$ dimensionless temperature, $\frac{T'-T_0}{T_{w1}-T_{w2}}$.

L characteristic length

Pr Prandtl number, $\nu/\alpha$
$k$ thermal conductivity
$Q$ dimensionless conduction heat flux, $Q'/Q_0$
$Q'$ conduction heat flux
$Q_o$ reference conduction heat flux
$p$ Laplacian domain
$t'$ time
$t$ dimensionless time, $\alpha t'/L^2$
$s$ suction/injection parameter, $v_0 L/\alpha$
$T'$ temperature
$T_0$ initial temperature
$T_{w1}$ hot wall temperature
$T_{w2}$ cold wall temperature
$U$ dimensionless velocity, $u'/u_0$
$u'$ axial velocity
$u_0$ reference velocity, $L^2 g\beta(T_w - T_0)/\alpha$
$V$ Laplace transformation of dimensionless heat flux
$W$ Laplace transformation of dimensionless temperature
$y$ transverse coordinate
$Y$ dimensionless transverse coordinate, $y/L$

**Greek symbols**
$\alpha$ thermal diffusivity
$\tau_q'$ phase-lag in heat flux vector
$\tau_q$ dimensionless phase-lag in heat flux vector, $\tau_q'\alpha/L^2$
$\tau_T'$ phase-lag in temperature gradient vector
$\tau_T$ dimensionless phase-lag in temperature gradient vector, $\tau_T'\alpha/L^2$
$\Omega$ $\frac{2-\sigma_v}{\sigma_v}$
$\Psi$ $\frac{2-\sigma_T}{\sigma_T}.\frac{2\gamma}{\gamma+1}$
$\sigma_v$ tangential-momentum accommodation coefficient
$\sigma_T$ thermal accommodation coefficient
$\gamma$ specific heat ratio
$\lambda$ mean free path
$v$ kinematic viscosity
$\mu$ coefficient of viscosity

**Acknowledgment**
The authors declare that they have no conflicts of interest in this research.

## REFERENCES

[1] Tzou, D. Y., (1995), *A unified approach for heat conduction from macro- to micro-scale* ASME, Journal of Heat Transfer, **117**, 8 – 16.

[2] Tzou, D. Y., (1997), *Macro- to Microscale Heat Transfer, The Lagging Behaviour*, Taylor and Francis, Washington DC, pp. 1 – 64.

[3] Quintanilla, R., and Rache, R., (2005), *Qualitative aspects in dual-phase-lag thermoelasticity*, Konstanzer Schriften in Mathematik und informatics, **206**, 1 – 28.

[4] Cattaneo, C., (1958), *A form of heat conduction equation which eliminates the paradox of instantaneous propagation*, Compte Rendus Acad. Sci. **247**:431 – 433.

[5] Vernotte, P., (1961), *Les paradoxes de la theorie continue de l'equation de la chaleur*, Compte Rendus, Acad. Sci. Vol. **246**: 3154 – 3155.

[6] Al-Nimr, A. A., and Naji, M., ($2000_a$), *The hypoberbolic heat conduction equation in an anisotropic material*, International Journal of Thermophysics, **21**, 281 – 287.

[7] Al-Nimr, A. A., and Naji, M., ($2000_b$), *On the Phase-lag effect on the nonequilibrium entropy production,* Microscale Thermophysics Eng. **4**, 231.

[8] Khadrawi, A. F., and Al-Nimir, M. A., (2007), *Unsteady Natural Convection Fluid Flow in a Vertical Microchannel under the Effect of the Dual-Phase-Lag Heat-Conduction Model*, International Journal of Thermophysics, Vol. **28**(4), 1387 – 1400.

[9] Khadrawi, A. F., Othman, A., and Al-Nimir, M. A., (2005), *Transient Free Convection Fluid in a vertical Microchannel as described by the Hyperbolic Heat Conduction Model*, Int. J. Thermophysics **26 (3)**, pp.905 – 918.

[10] Al-Nimr, M. A., and Khadrawi, A. F., (2004), *Thermal Behaviour of a Stagnant Gas Confined in a Horizontal Microchannel as Described by the Dual-Phase-Lag Heat Conduction Model*, International Journal of Thermophysics, Vol. **25**(6)**,** 1953 -1964.

[11] Ghazanfarian, J., and Abbassi, A., (2009), *Effect of boundary scattering on Dual-Phase-Lag model to simulate micro- and nano-scale heat conduction*, International Journal of Heat and Mass Transfer, **52**, pp. 3706 – 3711.

[12] Chen, G., (2001), *Ballistic-diffusive equations for Transient heat conduction from Nano to Microscale,* ASME Journal of Heat Transfer, **124**, pp. 320 – 328.

[13] Yang, R., Chen, G., Laroche, N., and Taur, Y., (2005), *Simulation nanoscale multidimensional transient heat conduction problem using ballistic diffusive equations and phonon Boltzann equation,* ASME, Journal of Heat Transfer **127** 298 – 306.

[14] Quintanilla, R., (2002), *experimental stability in the dual-phase-lag heat conduction theory*, Journal of Non-Equilibrium Thermodynamics, **27**, pp. 217 – 227.

[15] Basirat, H., Ghazanfarian, J., Foroogh, P., (2006) *Implementation of dual-phase-lag model at different Knudsen numbers within slab heat transfer*, in: Proceedings of the International Conference on Modelling and Simulation (MSO6), Konia, Turkey, pp. 895 – 899.

[16] Horgan, C. O., and Quintanilla, R., (2005), *Spatial behaviour of solutions of Dual-Phase-Lag heat conduction*, Math. Meth. Appl. Sci., **28**, pp. 43 – 57.

[17] Guo, Z. Y., and Li, Z. X., (2003), *Size Effect on Microscale Single-Phase flow and Heat Transfer*, International Journal of Heat Transfer, **46**, pp. 59-149.

[18] Eckert, E. R. G and Drake, R. M., (1972), *Analysis of heat and mass transfer*, New York: